GDCh Research Article Angewandte International Edition Chemie www.angewandte.org

How to cite: *Angew. Chem. Int. Ed.* **2025**, *64*, e202423809
doi.org/10.1002/anie.202423809

Porous Organic Polymers | Hot Paper

Porous Organic Polymers Incorporating Shape-Persistent Cyclobenzoin Macrocycles for Organic Solvent Separation

Timur Ashirov, Jay Lim, Alexandra Robles, Thamon Puangsamlee, Patrick W. Fritz, Aurelien Crochet, Xiqu Wang, Connor Hewson, Paul Iacomi, Ognjen Š. Miljanić, and Ali Coskun**

Abstract: The recovery and separation of organic solvents is highly important for the chemical industry and environmental protection. In this context, porous organic polymers (POPs) have significant potential owing to the possibility of integrating shape-persistent macrocyclic units with high guest selectivity. Here, we report the synthesis of a macrocyclic porous organic polymer (*np*-POP) and the corresponding model compound by reacting the cyclotetrabenzil naphthalene octaketone macrocycle with 1,2,4,5-tetraaminobenzene and 1,2-diaminobenzene, respectively, under solvothermal conditions. Co-crystallization of the macrocycle and the model compound with various solvent molecules revealed their size-selective inclusion within the macrocycle. Building on this finding, the *np*-POP with a hierarchical pore structure and a surface area of 579 $m^2 g^{-1}$ showed solvent uptake strongly correlated with their kinetic diameters. Solvents with kinetic diameters below 0.6 nm – such as acetonitrile and dichloromethane – showed high uptake capacities exceeding 7 $mmol\,g^{-1}$. Xylene separation tests revealed a high overall uptake (~34 wt %), with *o*-xylene displaying a significantly lower uptake (~10 wt % less than other isomers), demonstrating the possibility of size and shape selective separation of organic solvents.

[*] Dr. T. Ashirov, Dr. P. W. Fritz, Dr. A. Crochet, Prof. A. Coskun
Department of Chemistry, University of Fribourg,
Chemin du Musée 9, CH-1700 Fribourg, Switzerland
E-mail: ali.coskun@unifr.ch

J. Lim, Dr. A. Robles, Dr. T. Puangsamlee, Dr. X. Wang, Prof. O. Š. Miljanić
Department of Chemistry, University of Houston,
3585 Cullen Boulevard #112 Houston, TX 77204-5003, United States
E-mail: miljanic@uh.edu

C. Hewson, Dr. P. Iacomi
Surface Measurement Systems Ltd.
5 Wharfside, Rosemont Road, Alperton,
Middlesex, HA0 4PE, United Kingdom

Prof. O. Š. Miljanić
Faculty of Chemical Engineering,
Industrial University of Ho Chi Minh City,
Ho Chi Minh City, 71408, Vietnam

Introduction

Porous organic polymers (POPs) are a promising class of materials capable of addressing environmental and industrial challenges, particularly in the areas of separation, capture, and selective isolation of pollutants.[1] POPs have already found applications ranging from the capture of carbon dioxide (CO_2)[2] and chlorofluorocarbons (CFCs)[1c,3] to the extraction of organic dyes,[4] heavy metals from wastewater,[5] and radioactive iodine from nuclear waste.[6] These capabilities have established POPs as a promising alternative to conventional porous materials such as activated carbon, primarily due to their tunable porosity, high surface area, and customizable chemical functionalities.

In recent years, there has been increased focus on tuning the properties of POPs for separation applications through structural control aimed at improving their selectivity, stability, and overall performance. Among the design strategies, the incorporation of shape-persistent macrocycles and molecular cages into the POP networks has been particularly effective.[7] Macrocycles, cages, and other shape-persistent molecules exhibit unique structural features that enable enhanced host–guest interactions in solution, which can be transferred into the solid state by integrating them into the polymer networks for the selective capture and separation of small molecules.[7–8] In this direction, a macrocyclic cyclotetrabenzoin octaketone, synthesized by Miljanić and colleagues, has proven to be an excellent host for small molecules, demonstrating its ability to effectively separate CO_2 from nitrogen (N_2),[8a,b,9] underscoring the potential of these macrocycles as monomeric units for the synthesis of POPs for diverse separation applications. Macrocyclic POPs are quite promising for organic solvent separation owing to their stability, selective adsorption properties, and molecular sieving abilities.[7b,10] Organic solvent separation, recovery, and removal are critically important in the chemical, pharmaceutical, and petrochemical industries.[11] In this context, cyclotetrabenzil derivatives have already been demonstrated as hosts for small linear solvent molecules such as carbon disulfide (CS_2), MeCN, and propargyl alcohol.[9a,b] In order to expand the scope of accessible guest molecules, here we synthesized a larger cyclotetrabenzil octaketone based on the 2,6-disubstituted naphthalene skeleton (naphthaketone), which features a distinct square-shaped cavity with a width of 8.6 Å (Scheme 1a). The incorporation of naphthalene moiety into the macrocyclic

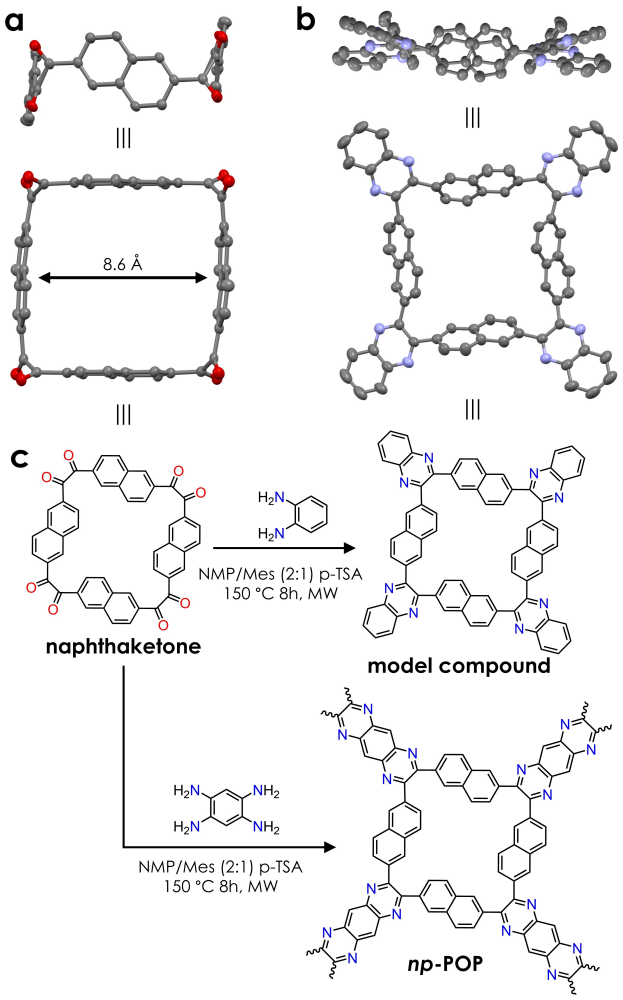

Scheme 1. Top and side views of single-crystal X-ray structures of (a) naphthaketone and (b) the model compound. Solvent molecules are omitted for clarity. (c) The synthesis of the model compound and *np*-POP under solvothermal conditions. Abbreviations: NMP: *N*-methyl-2-pyrrolidone, Mes: mesitylene, *p*-TSA: *p*-toluenesulfonic acid, MW: microwave.

framework introduces several key advantages, most notably the larger pore size compared to the one in the phenyl-based analog; such larger pores are beneficial for accommodating a wider range of molecules.[9a] Additionally, the rigid aromatic structure of naphthalene, coupled with its π-conjugation, significantly enhances the interaction between the macrocycle and target organic solvents, which was verified by the co-crystallization of the macrocycle with various solvents, thus improving both the selectivity and the separation efficiency of the material for organic solvent capture/separation applications.[12] The naphthaketone macrocycle, with its rigid core and larger pore size, presents a promising alternative for selective solvent separation by accommodating various solvent molecules based on their sizes and affinities.[9b,12] Accordingly, we synthesized a macrocyclic porous organic polymer incorporating naphthaketone macrocycles, called *np*-POP, for organic solvent separation. The synthesized *np*-POP exhibited a surface area of 579 $m^2 g^{-1}$, featuring two distinct types of pores with 0.58 and 0.96 nm in size that belong to the macrocyclic cavity and porosity formed as a result of polymerization, respectively. Our results demonstrated a clear correlation between the kinetic diameters of solvents and their gravimetric uptake capacities. Specifically, we found that molecules with kinetic diameters smaller than ~0.58 nm are adsorbed in both the primary and the secondary pores, whereas larger molecules—such as toluene and xylenes—could only access the secondary pores formed during the polymerization process. We also observed a difference in uptake capacity between *m*-, *p*-, and *o*-xylene. These results showcase the solvent separation capability of *np*-POP based on size and shape selectivity.

Results and Discussion

The naphthaketone macrocycle was synthesized by following previously published procedures, starting from 2,6-naphthalene dialdehyde in a two-step process (refer to the Supporting Information for experimental details).[9a,12–13] The single-crystal X-ray diffraction (SCXRD) structure of naphthaketone revealed a square-shaped cavity measuring 8.6×8.6 Å. The crystal structure further indicates that the compound adopts a chair-like conformation, in which one pair of naphthalenes is oriented face-to-face. The carbonyl pairs on the other hand are positioned perpendicular to one another with an O=C–C=O dihedral angle of ~89° (Scheme 1a).

To verify the host–guest interactions of naphthaketone with different solvent molecules, we co-crystallized the macrocycle with several commonly used solvents. SCXRD structures revealed that solvents such as chloroform and 1,4-dioxane could easily be accommodated within the naphthaketone cavity (Figure 1a, b), demonstrating its ability to host small molecules, with chloroform fitting particularly well due to its small kinetic diameter of 0.54 nm. Co-crystals of the macrocycle were incidentally obtained with chloroform during the single-crystal growth process for *p*-dimethoxybenzene (Figure 1a). Following this observation, we explored the interaction of the macrocycle with various aromatic solvents. Even though the naphthaketone cavity was large enough to host *m*-dichlorobenzene (*m*-DCB), the side-on [π···π] stacking interactions between the *m*-DCB and the naphthalene units dominated, causing the guest molecule to align with the naphthalene moiety outside the cavity, with the benzene-naphthalene centroid-to-centroid distance of 3.77 Å suggesting strong [π···π] stacking interactions (Figure 1c). The solvents with larger kinetic diameters, such as 1,2,4-trichlorobenzene (1,2,4-TCB), were too bulky to fit within the cavity. Instead, they formed side-on [π···π] stacking interactions with the naphthalene units (Figure 1d). Attempts to grow single crystals with 1,2,4-TCB using a 1:1 mixture of 1,4-dioxane and hexane resulted in co-crystals where dioxane occupied the central cavity of the macrocycle, thus demonstrating the ability of the macrocycle to distinguish between aliphatic and aromatic solvents.

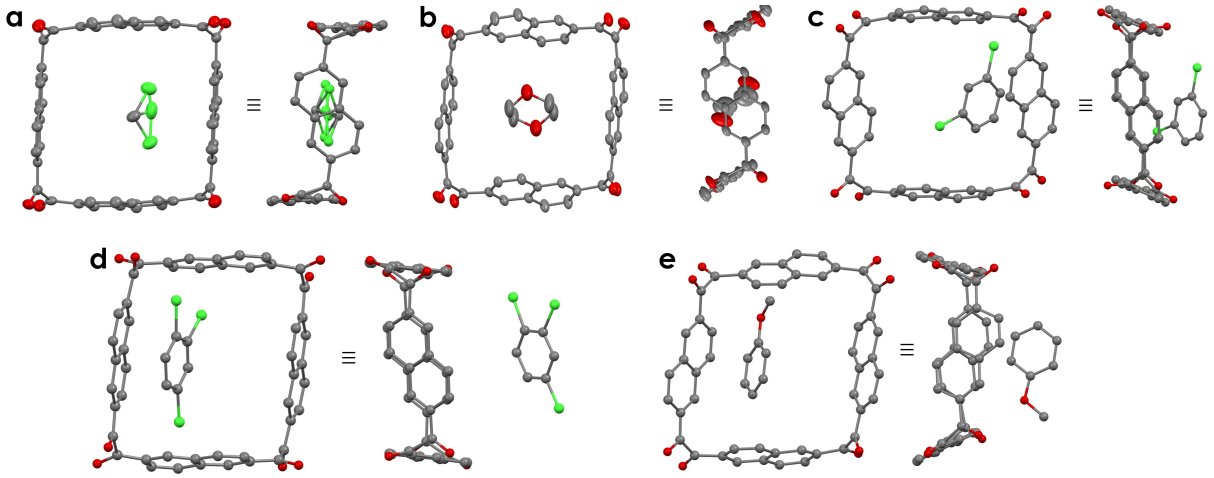

Figure 1. SCXRD crystal structures of naphthaketone with (a) chloroform (as the chloroform molecule is disordered over two symmetry-related positions, only one of them is shown for clarity), (b) 1,4-dioxane, (c) *m*-DCB, (d) 1,2,4-TCB, and (e) methoxybenzene.

Co-crystals of the naphthaketone macrocycle and methoxybenzene were also obtained (Figure 1e). In this case, short contacts were predominantly observed between the macrocycle's hydrogen atoms and the oxygen atom of the methoxybenzene, indicating a different interaction mechanism from the previously studied chlorinated solvents. These crystallization experiments also demonstrated the size-dependent selectivity of the naphthaketone macrocycle towards smaller aliphatic organic solvents, while larger aromatic molecules tend to form side-on interactions rather than occupying the cavity. Encouraged by these results, we synthesized a naphthaketone-based porous organic polymer (*np*-POP) by reacting naphthaketone with 1,2,4,5-tetraaminobenzene tetrahydrochloride (TABH) under solvothermal conditions using an MW reactor. The reaction was carried out in a 2:1 mixture of *N*-methyl-2-pyrrolidone, NMP, and mesitylene in the presence of *p*-toluenesulfonic acid, *p*-TSA, as a catalyst (Scheme 1c).[14] After 8 h at 150 °C in the MW, the *np*-POP was successfully isolated by filtration and washed with methanol, tetrahydrofuran, and acetone (see Supporting Information for experimental details). We also synthesized a model compound under the same conditions using 1,2-phenylenediamine as the reactant. The SCXRD crystal structure of the model compound was obtained by the slow diffusion of ethyl acetate into a chloroform solution of the model compound. Interestingly, the SCXRD crystal structure revealed that the model compound adopts a two-dimensional structure, unlike the smaller octaketone macrocycle (Scheme 1b).[8a,13] This is likely due to the rigid structure of the naphthaketone, which prevents significant rearrangement and helps preserve the cavity.[12] We also observed a packing arrangement featuring one-dimensional channels formed by the alignment of macrocycle cavities (Figure 2a). accommodating ethyl acetate molecules (Figure 2b). The presence of ethyl acetate over chloroform can be attributed to the former's smaller kinetic diameter of ~0.46 nm.[15] These findings further demonstrate that the cavity of cyclobenzoin is still preserved after post-functionalization for solvent separation, thus providing valuable insights toward understanding the solvent uptake mechanism in *np*-POP.

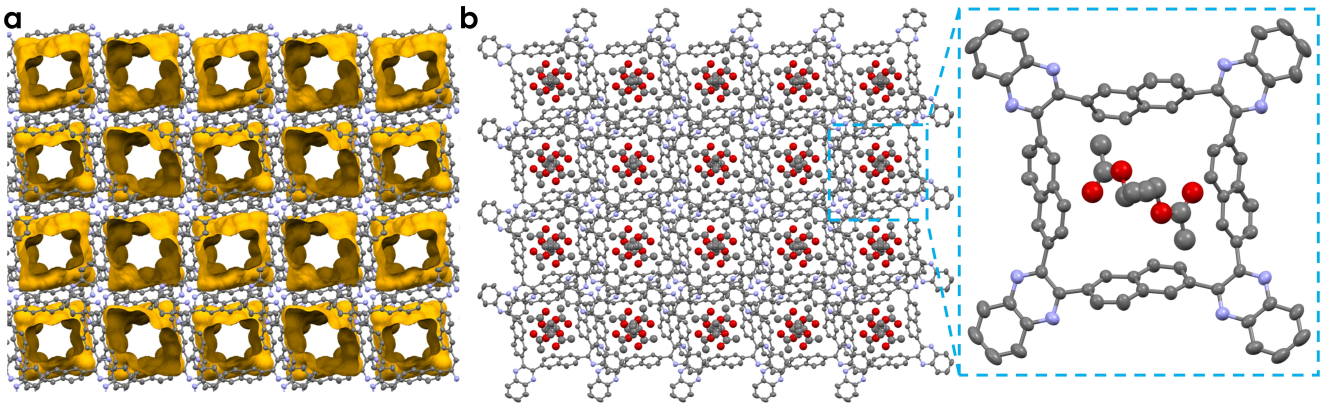

Figure 2. SCXRD crystal structure of the model compound revealing (a) its porosity and (b) the inclusion of ethyl acetate (EA) solvent molecules inside the pores. Two EA molecules can fit inside the square-shaped pore of the model compound.

The successful formation of the *np*-POP was confirmed through Fourier transform infrared (FTIR) spectroscopy (Figure 3a). The disappearance of characteristic $-NH_3^+$ bending vibrations of TABH at ~2466 cm^{-1} and –C–N– vibrations at ~1219 cm^{-1}, along with the appearance of new –C=N– vibrations at ~1672 and 1625 cm^{-1} in the *np*-POP FTIR spectrum support the polymerization process.[8a,9d] Additionally, the decreased intensity of the –C=O vibrations of naphthaketone at ~1673 cm^{-1} further corroborates the formation of the polymer (Figure 2a).

The chemical structure of *np*-POP was further characterized using X-ray photoelectron spectroscopy (XPS). The survey spectra revealed the composition to be 76.5 % C, 9.0 % N, and trace amounts of metal impurities, likely originating from the support (Figure S3, Table S1, Supporting Information). The detected oxygen was mostly attributed to the carbonyl end groups of the polymer network (Figure S4, Table S4). In the high-resolution C1s XPS spectrum, four main types of carbon binding energies were identified at 284.8, 285.7, 286.5, and 288.1 eV, corresponding to –C–C–/–C=C–,[16] –C–N–/C=N–,[8a,17] –C–O– and –C=O, respectively (Table S2). Similarly, the high-resolution N1s spectrum of *np*-POP showed two primary nitrogen environments at 398.8 and 400.6 eV, which were attributed to –C–N–/–C=N– and graphitic nitrogen, respectively (Table S3).[17] Further analysis of the *np*-POP using solid-state cross-polarization ^{13}C magic angle spinning (CP-MAS) nuclear magnetic resonance (NMR) spectroscopy revealed three broad peaks: at 129.4 ppm, corresponding to the carbon atoms of the naphthalene moiety, at broad peak 150.8–154.3 ppm, representing carbons bound to nitrogen atoms, and at 194.8 ppm, indicative of –C=O end-groups (Figure S5). The atomic composition of *np*-POP was further examined using elemental analysis, which revealed the presence of 73.56 % carbon and 10.84 % nitrogen (Table S1). Powder X-ray diffraction (XRD) analysis of *np*-POP revealed its amorphous nature (Figure S6). Thermogravimetric analysis (TGA) of *np*-POP showed that the material remained thermally stable up to 450 °C under air, confirming the robustness of its structure (Figure S7). The residual mass after TGA was attributed to incomplete combustion.[18]

The porosity of *np*-POP was investigated using nitrogen (N_2) sorption at 77 K, and the specific surface area was calculated based on the Brunauer–Emmett–Teller (BET) theory[19] (Figure S8). The *np*-POP exhibited a BET surface area of 579 $m^2 g^{-1}$, with a pore volume of 0.28 $cm^3 g^{-1}$ (Table S5). The N_2 adsorption isotherm showed a Type I profile, characteristic of a microporous material (Figure 4a). The broad hysteresis in the desorption branch over the entire pressure range was attributed to the swelling of the polymer network. Pore size analysis using non-local density functional theory (NLDFT) with a heterogeneous surface model revealed two main pore types. The first type of pores, with a diameter of ~0.58 nm, corresponds to the intrinsic macrocycle pore, while the larger second pore, with a diameter of ~0.95 nm, formed in the polymerization process (Figure 4b). Additionally, the Barrett–Joyner–Halenda (BJH) model[20] indicated the presence of mesopores (Figure S9). In line with previously reported cyclotetrabenzil-based POPs,[8a,9d] the *np*-POP demonstrated a CO_2 uptake capacity of 2.6 mmol g^{-1} at 273 K and 1.1 bar (Figure S10), further highlighting its microporosity and the potential for other gas sorption applications like carbon capture.

After confirming the successful synthesis of *np*-POP and analyzing its porosity, we evaluated its vapour sorption properties. To comprehensively explore the effect of guest

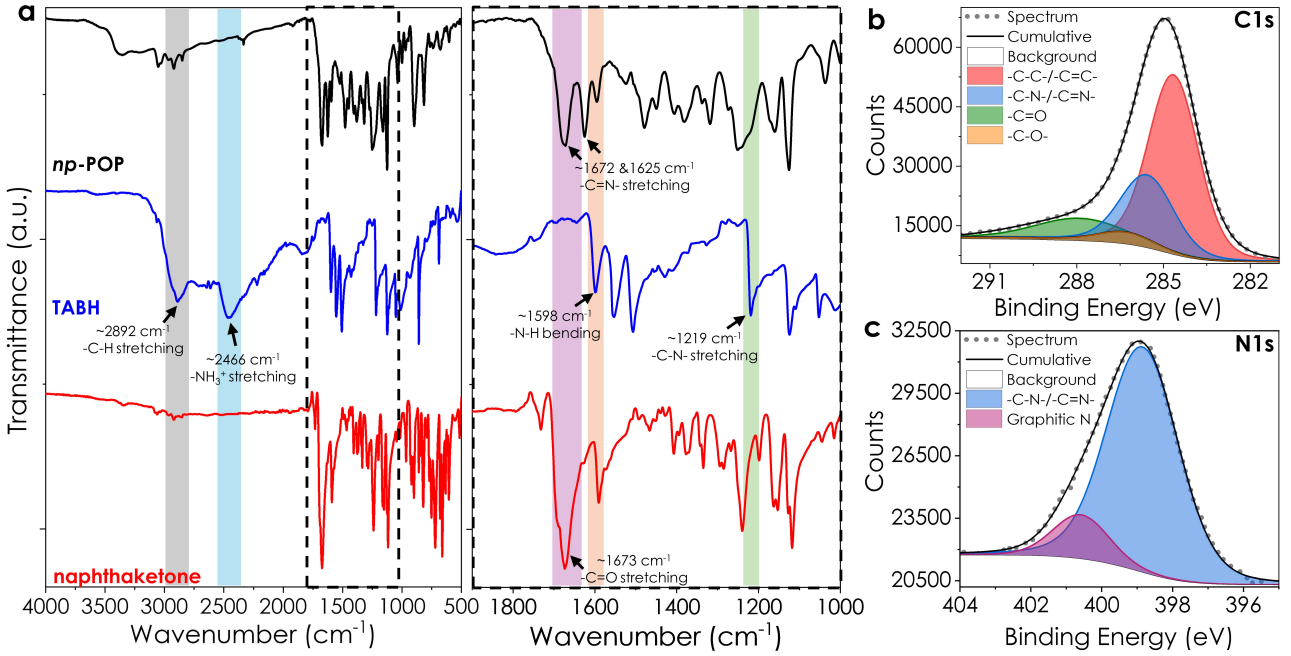

Figure 3. Characterization of *np*-POP: (a) FTIR spectra of *np*-POP in comparison with the starting materials, with the key vibration bands highlighted. High-resolution XPS (b) C1s and (c) N1s spectra of *np*-POP.

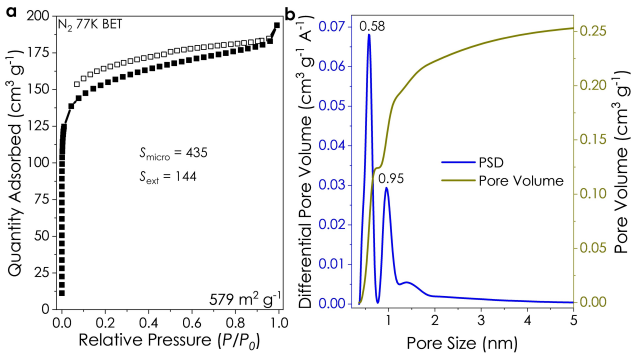

Figure 4. Porosity analysis of *np*-POP: (a) N_2 uptake isotherm of *np*-POP measured at 77 K. The filled and empty symbols represent adsorption and desorption branches, respectively. (b) NLDFT pore size distribution of *np*-POP.

nature on the uptake and consequent guest-host interactions, we selected three classes of solvents for this study: (1) polar non-aromatic molecules: acetonitrile, methylene chloride, chloroform, and 1,4-dioxane, (2) aromatic molecules: toluene, xylenes, and mesitylene, and (3) aliphatic hydrocarbons: hexane, cyclohexane, iso-octane. Solvent uptake capacities were measured using a gravimetric vapor sorption technique (DVS, Figures S11–S22, Supporting Information). Sorption kinetics and isotherms were obtained by recording the continuous weight change of the sample at constantly maintained relative pressure steps (Figure 5a). The resulting isotherms show a Langmuir-like type-I behavior. Notably, they are characterized by a pronounced hysteresis. A closer look at the time-resolved kinetic data (Figures S11–S22) demonstrates slow sorption kinetics. This observation can indicate that sorption is a diffusion-limited process or that it is associated with structural flexibility and framework reorganization.

The analysis of the solvent interactions with *np*-POP revealed important trends. By correlating the total solvent uptake capacities with the kinetic diameters of the solvents (Figure 5b), we found a clear relationship between molecular size and uptake. Acetonitrile and dichloromethane, with kinetic diameters of 0.34 nm and 0.46 nm, respectively, exhibited the highest uptake capacities, exceeding 7 mmol g^{-1} (Table 1). Larger solvents, such as chloroform and 1,4-dioxane, with their respective kinetic diameters of 0.54 and 0.55 nm also showed significant uptake capacities above 5 mmol g^{-1}. Based on SCXRD crystal structures (Figure 1), we infer that these solvents are absorbed into both the primary and secondary pores of the polymer. The high uptake of 1,4-dioxane suggests potential applications for *np*-POP in separating dioxane-water mixtures, which are particularly challenging due to the formation of an azeotrope with ~18 % water.[21]

Aromatic solvents displayed uptake capacities below 4 mmol g^{-1}, following the same uptake capacity vs. kinetic diameter trend (Figure 5b). This decrease in uptake is attributed to the larger kinetic diameters of these molecules, which exceed the size of the primary pore (~0.58 nm), relegating them to the secondary pores. Additionally, due to the aromatic nature of these solvents, [π···π] interactions play a dominant role in their adsorption behavior, influencing both their packing in the secondary pores and uptake kinetics, as corroborated by the SCXRD structures (Figure 2). Interestingly, when analyzing xylene isomers, we found that *m*- and *p*-xylenes exhibited similar uptake capacities of approximately 3.2 mmol g^{-1} (~34 wt %), whereas *o*-xylene showed a noticeably lower uptake of 2.6 mmol g^{-1} (Table 1). This 10 wt % uptake difference (Figure S23) can be attributed to *o*-xylene's larger kinetic diameter and poorer packing efficiency compared to *m*- and *p*-xylenes.[22] These results highlight the potential of *np*-POP for selectively separating *m*- and *p*-xylene, which exhibit

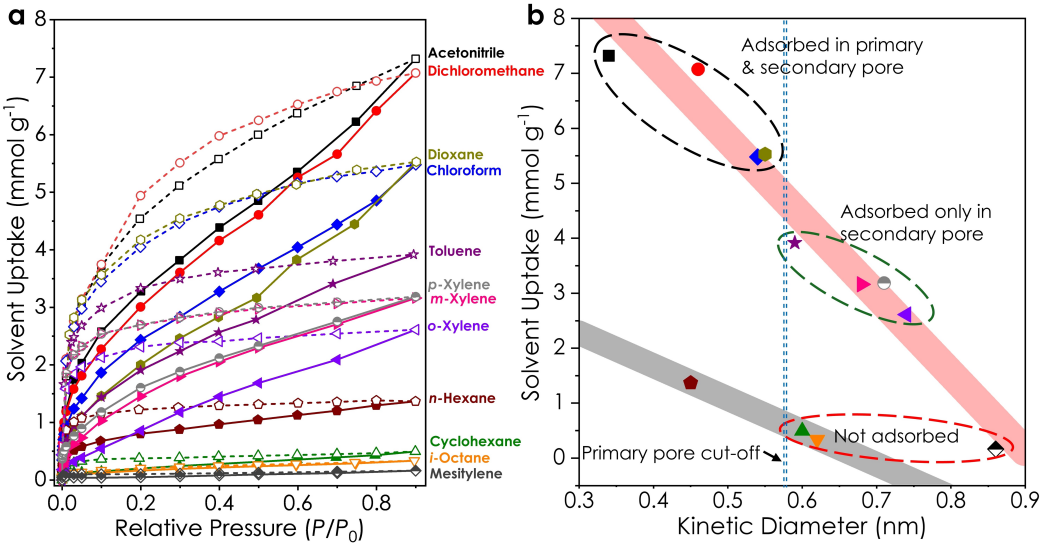

Figure 5. Solvent uptake performance of *np*-POP: (a) Solvent uptake isotherm of *np*-POP. Filled and empty symbols represent adsorption and desorption branches, respectively. (b) Correlation of solvent uptake capacities vs kinetic diameter of solvents.

Table 1: Solvent parameters and uptake values for *np*-POP.

Solvent	Kinetic Diameter (nm)	Uptake (mmol g^{-1})	
Acetonitrile	0.34[25]	7.32	Adsorbed in primary & secondary pore
Dichloromethane	0.46[26]	7.07	
Chloroform	0.54[27]	5.48	
1,4-Dioxane	0.55[28]	5.53	
Toluene	0.59[29]	3.92	Adsorbed mainly in secondary pore
m-Xylene	0.68[22a]	3.16	
p-Xylene	0.71[22a]	3.18	
o-Xylene	0.74[22a]	2.61	
n-Hexane	0.45[30]	1.37	
Cyclohexane	0.60[31]	0.49	Not adsorbed
i-Octane	0.62[29]	0.34	
Mesitylene	0.86[29]	0.16	

comparable uptake capacities above 30 wt %, from *o*-xylene.[10b,23] The critical role of the kinetic diameter of solvents is further corroborated by the negligible uptake of mesitylene, which showed almost no weight change (Figure S19). Despite mesitylene's smaller kinetic diameter (0.86 nm) relative to the 0.95 nm secondary pore, its bulky structure and steric hindrance prevent efficient packing and uptake.[24] The solvent uptake performance of *np*-POP was highly competitive compared to other porous materials (Table S6).

The solvent uptake capacities versus kinetic diameter followed a linear trend. Interestingly, hydrocarbons deviated significantly from this trend. For example, hexane exhibited an uptake capacity of only ~1.4 mmol g^{-1}, despite having a kinetic diameter similar to dichloromethane (Table 1). This deviation is likely due to the bulkiness of hydrocarbons and the consequent limitations in mass transport kinetics. *Iso*-octane showed no measurable uptake, and cyclohexane exhibited a very low capacity as well (Table 1). These findings suggest that hydrocarbons are hindered by both pore geometry and packing inefficiencies. The uptake capacities of hydrocarbons follow their own linear trend, and their uptake capacity is more than three times lower than that of other solvents.

To evaluate the repeatability of the *np*-POP's solvent separation performance, we measured the uptake of xylene isomers after regenerating the samples at 120 °C for 5 hours under vacuum (Figures S24–S26). Although the adsorption capacities showed a slight decrease (~3–4 %), suggesting that a longer regeneration time is required, the selectivity trend remained unchanged; *o*-xylene continued to exhibit significantly lower uptake compared to *p*- and *m*-xylenes (Figure S27). We also tested the chemical stability of *np*-POP by immersing it in *N*,*N*-dimethyl formamide (DMF) at 100 °C for 24 h. The FTIR spectra showed no significant change while the N_2 sorption at 77 K showed an identical Type I isotherm with a slightly lower surface area indicating some of the micropores are occupied by DMF molecules (Figure S28), thus confirming the stability of *np*-POP under harsh conditions.

The desorption branch in the N_2 isotherm (Figure 4a) exhibited a broad hysteresis in the entire pressure range, an indication of the swelling of the polymer network. To understand the impact of swelling on the solvent uptake performance of *np*-POP, we calculated the pore volume by dividing the gravimetric uptake capacity of the solvents by the solvent density based on the assumption that the density of the solvent in the pores will be the same as the one with the bulk. While the pore volume determined from N_2 uptake at 77 K was 0.28 cm^3 g^{-1} (Table S5), the pore volume calculated using dichloromethane uptake increased to 0.45 cm^3 g^{-1}, indicating network swelling in the presence of solvents. The highest pore volume was observed with 1,4-dioxane (0.47 cm^3 g^{-1}), confirming that the extent of network swelling depends on the guest molecule. Swelling of the polymer network is expected to further increase the accessibility of the primary pores. These results demonstrate that macrocyclic porous organic polymers like *np*-POP can be excellent candidates for solvent separation by leveraging the intrinsic properties of the macrocycle to target specific solvent classes.

Conclusion

We demonstrated that the intrinsic properties of cyclotetrabenzil-based macrocycles can be transferred into a porous organic polymer, resulting in superior performance in solvent separation, and offering improved selectivity, thermal stability, and chemical robustness. The distinct pore structure and various noncovalent interactions enabled selective uptake of small solvents, with a strong correlation between the kinetic diameter of solvents and their uptake capacities. This study highlights the potential of macrocyclic frameworks in advancing solvent separation technologies and contributes to the growing body of knowledge on functionalized POPs for environmental and industrial applications.

Supporting Information

Deposition Numbers 2406414 (for Model Compound), 2406415 (for methoxybenzene in naphthaketone), 2406416

(for *o*-DCB in naphthaketone), 2406417 (for chloroform in naphthaketone), 2406418 (for 1,2,4-TCB and 1,4-dioxane in naphthaketone) contains the supplementary crystallographic data for this paper. These data are provided free of charge by the joint Cambridge Crystallographic Data Centre (CCDC). The authors have cited additional references within the Supporting Information.[9a,12–14,22,23c,32]

Acknowledgements

A.C. acknowledges the NCCR Catalysis (grant number 180544), a National Centre of Competence in Research funded by the Swiss National Science Foundation. A.C. also acknowledges FriMat at the University of Fribourg. O.Š.M. acknowledges the support of the Welch Foundation (grant E-2205-20240404) and the US National Science Foundation (grant CHE-2204236).

Conflict of Interest

The authors declare no conflict of interest.

Data Availability Statement

The data that support the findings of this study are openly available in Zenodo at https://zenodo.org/records/14639311, reference number zenodo.14639311.

.

Keywords: cyclotetrabenzoins · macrocyclic porous organic polymers · solvent separation · host–guest chemistry · naphthalene macrocycles

[1] a) Y. Song, J. Phipps, C. Zhu, S. Ma, *Angew. Chem. Int. Ed.* **2023**, *62*, e202216724; b) S. Fajal, S. Dutta, S. K. Ghosh, *Mater. Horiz.* **2023**, *10*, 4083–4138; c) Y.-L. Zhao, X. Zhang, M.-Z. Li, J.-R. Li, *Chem. Soc. Rev.* **2024**, *53*, 2056–2098.

[2] a) K. S. Song, P. W. Fritz, A. Coskun, *Chem. Soc. Rev.* **2022**, *51*, 9831–9852; b) D. Luo, T. Shi, Q.-H. Li, Q. Xu, M. Strømme, Q.-F. Zhang, C. Xu, *Angew. Chem. Int. Ed.* **2023**, *62*, e202305225; c) P. Bhanja, A. Modak, A. Bhaumik, *ChemCatChem* **2019**, *11*, 244–257.

[3] a) Z. Zhang, O. Š Miljanić, *Org. Mater.* **2019**, *01*, 019–029; b) K. Tian, S. M. Elbert, X.-Y. Hu, T. Kirschbaum, W.-S. Zhang, F. Rominger, R. R. Schröder, M. Mastalerz, *Adv. Mater.* **2022**, *34*, 2202290.

[4] J. Byun, H. A. Patel, D. Thirion, C. T. Yavuz, *Nat. Commun.* **2016**, *7*, 13377.

[5] a) K. S. Song, A. Coskun, *Chimia* **2023**, *77*, 122–126; b) Y. Hong, D. Thirion, S. Subramanian, M. Yoo, H. Choi, H. Y. Kim, J. F. Stoddart, C. T. Yavuz, *Proc. Natl. Acad. Sci. USA* **2020**, *117*, 16174–16180.

[6] a) D. Shetty, J. Raya, D. S. Han, Z. Asfari, J.-C. Olsen, A. Trabolsi, *Chem. Mater.* **2017**, *29*, 8968–8972; b) T. Ashirov, K. S. Song, A. Coskun, *ACS Appl. Nano Mater.* **2022**, *5*, 13711–13719; c) W. Xie, D. Cui, S.-R. Zhang, Y.-H. Xu, D.-L. Jiang, *Mater. Horiz.* **2019**, *6*, 1571–1595.

[7] a) Z. Li, Y.-W. Yang, *Adv. Mater.* **2022**, *34*, 2107401; b) T. Skorjanc, D. Shetty, A. Trabolsi, *Chem* **2021**, *7*, 882–918; c) W. Zhou, R. Lavendomme, D. Zhang, *Chem. Commun.* **2024**, *60*, 779–792.

[8] a) T. Ashirov, M. Alrayyani, K.-S. Song, O. Š Miljanić, A. Coskun, *Org. Mater.* **2021**, *03*, 346–352; b) Y.-T. Wang, C. McHale, X. Wang, C.-K. Chang, Y.-C. Chuang, W. Kaveevivitchai, O. Š Miljanić, T.-H. Chen, *Angew. Chem. Int. Ed.* **2021**, *60*, 14931–14937; c) X.-Y. Lou, S. Zhang, Y. Wang, Y.-W. Yang, *Chem. Soc. Rev.* **2023**, *52*, 6644–6663.

[9] a) A. M. Eisterhold, T. Puangsamlee, S. Otterbach, S. Bräse, P. Weis, X. Wang, K. V. Kutonova, O. Š Miljanić, *Org. Lett.* **2021**, *23*, 781–785; b) C. M. McHale, C. R. Stegemoller, M. I. Hashim, X. Wang, O. Š Miljanić, *Cryst. Growth Des.* **2019**, *19*, 562–567; c) Y.-T. Wang, S. Jalife, A. Robles, M. Đerić, J. I. Wu, W. Kaveevivitchai, O. Š Miljanić, T.-H. Chen, *ACS Appl. Nano Mater.* **2022**, *5*, 14021–14026; d) T. Ashirov, T. Puangsamlee, A. Robles, P. W. Fritz, K. Piech, O. Š Miljanić, A. Coskun, *Helv. Chim. Acta* **2023**, *106*, e202300072.

[10] a) W. Chen, P. Chen, G. Zhang, G. Xing, Y. Feng, Y.-W. Yang, L. Chen, *Chem. Soc. Rev.* **2021**, *50*, 11684–11714; b) G. Zhang, Y. Ding, A. Hashem, A. Fakim, N. M. Khashab, *Cell Rep. Phys. Sci.* **2021**, *2*, 100470.

[11] a) P. Marchetti, M. F. Jimenez Solomon, G. Szekely, A. G. Livingston, *Chem. Rev.* **2014**, *114*, 10735–10806; b) C. Wang, C. Li, E. R. C. Rutledge, S. Che, J. Lee, A. J. Kalin, C. Zhang, H.-C. Zhou, Z.-H. Guo, L. Fang, *J. Mater. Chem. A* **2020**, *8*, 15891–15899; c) B. Liang, X. He, J. Hou, L. Li, Z. Tang, *Adv. Mater.* **2019**, *31*, 1806090.

[12] J. Meng, A. Robles, S. Jalife, W. Ren, Y. Zhang, L. Zhao, Y. Liang, J. I. Wu, O. Š Miljanić, Y. Yao, *Angew. Chem. Int. Ed.* **2023**, *62*, e202300892.

[13] S. Hahn, M. Alrayyani, A. Sontheim, X. Wang, F. Rominger, O. Š Miljanić, U. H. F. Bunz, *Chem. Eur. J.* **2017**, *23*, 10543–10550.

[14] H. Wei, S. Chai, N. Hu, Z. Yang, L. Wei, L. Wang, *Chem. Commun.* **2015**, *51*, 12178–12181.

[15] B. Zheng, L. L. Wang, L. Du, Y. Pan, Z. Lai, K. W. Huang, H. L. Du, *Mater. Horiz.* **2016**, *3*, 355–361.

[16] P. W. Fritz, T. Chen, T. Ashirov, A.-D. Nguyen, M. Dincă, A. Coskun, *Angew. Chem. Int. Ed.* **2022**, *61*, e202116527.

[17] D. Deng, X. Pan, L. Yu, Y. Cui, Y. Jiang, J. Qi, W.-X. Li, Q. Fu, X. Ma, Q. Xue, G. Sun, X. Bao, *Chem. Mater.* **2011**, *23*, 1188–1193.

[18] T. Ashirov, P. W. Fritz, T. Yildirim, A. Coskun, *Chem. Commun.* **2024**, *60*, 2657–2660.

[19] S. Brunauer, P. H. Emmett, E. Teller, *J. Am. Chem. Soc.* **1938**, *60*, 309–319.

[20] E. P. Barrett, L. G. Joyner, P. P. Halenda, *J. Am. Chem. Soc.* **1951**, *73*, 373–380.

[21] a) K. J. Godri Pollitt, J.-H. Kim, J. Peccia, M. Elimelech, Y. Zhang, G. Charkoftaki, B. Hodges, I. Zucker, H. Huang, N. C. Deziel, K. Murphy, M. Ishii, C. H. Johnson, A. Boissevain, E. O'Keefe, P. T. Anastas, D. Orlicky, D. C. Thompson, V. Vasiliou, *Sci. Total Environ.* **2019**, *690*, 853–866; b) A. Broughton, A. Sepulveda, K. Foster, T. Kruk, M. G. Nickelsen, M. Gillan, T. K. G. Mohr, *Remediation J.* **2019**, *29*, 49–63; c) T. Mahdi, A. Ahmad, M. M. Nasef, A. Ripin, *Sep. Purif. Rev.* **2015**, *44*, 308–330.

[22] a) J. Liu, M. Dong, Z. Sun, Z. Qin, J. Wang, *Colloids Surf. A Physicochem. Eng. Asp.* **2004**, *247*, 41–45; b) R. Lyndon, J. Bacsa, M. L. Jue, R. P. Lively, *Cryst. Growth Des.* **2018**, *18*, 2890–2898.

[23] a) G. Zhang, W. Lin, F. Huang, J. Sessler, N. M. Khashab, *J. Am. Chem. Soc.* **2023**, *145*, 19143–19163; b) S. H. Kim, J. H. Park, E. M. Go, W.-S. Kim, S. K. Kwak, *J. Ind. Eng. Chem.* **2020**, *85*, 276–281; c) Q. Wang, Y. Li, Z. Qiu, D. Zhou, L.

Yang, X. Suo, X. Cui, H. Xing, *Angew. Chem. Int. Ed.* **2024**, *63*, e202408817.
[24] P. A. Russo, M. M. L. R. Carrott, P. J. M. Carrott, *New J. Chem.* **2011**, *35*, 407–416.
[25] X. Li, Y. Liu, Q. Liu, Z. Zheng, H. Guo, *RSC Adv.* **2022**, *12*, 7189–7198.
[26] S. H. Madani, A. Silvestre-Albero, M. J. Biggs, F. Rodríguez-Reinoso, P. Pendleton, *ChemPhysChem* **2015**, *16*, 3984–3991.
[27] C. Carrara, G. Pagès, C. Delaurent, S. Viel, S. Caldarelli, *J. Phys. Chem. C* **2011**, *115*, 18776–18781.
[28] Q. W. Yeang, A. B. Sulong, S. H. Tan, *Sep. Purif. Technol.* **2018**, *192*, 240–252.
[29] J. Jae, G. A. Tompsett, A. J. Foster, K. D. Hammond, S. M. Auerbach, R. F. Lobo, G. W. Huber, *J. Catal.* **2011**, *279*, 257–268.
[30] F. Jiménez-Cruz, G. C. Laredo, *Fuel* **2004**, *83*, 2183–2188.
[31] F. D. Magalhães, R. L. Laurence, W. C. Conner, *J. Phys. Chem. B* **1998**, *102*, 2317–2324.
[32] a) O. V. Dolomanov, L. J. Bourhis, R. J. Gildea, J. A. K. Howard, H. Puschmann, *J. Appl. Crystallogr.* **2009**, *42*, 339–341; b) G. Sheldrick, *Acta Crystallogr. Sect. A* **2015**, *71*, 3–8; c) G. Sheldrick, *Acta Crystallogr. Sect. C* **2015**, *71*, 3–8; d) M. A. M. Alrayyani, Ph.D. thesis, *University of Houston* **2020**; e) L. Pan, Q. Chen, J.-H. Zhu, J.-G. Yu, Y.-J. He, B.-H. Han, *Polym. Chem.* **2015**, *6*, 2478–2487; f) X.-S. Wang, J. Liu, J. M. Bonefont, D.-Q. Yuan, P. K. Thallapally, S. Ma, *Chem. Commun.* **2013**, *49*, 1533–1535; g) K.-J. Oh, D.-W. Park, S.-S. Kim, S.-W. Park, *Korean J. Chem. Eng.* **2010**, *27*, 632–638; h) S. Kim, D. Thirion, T. S. Nguyen, B. Kim, N. A. Dogan, C. T. Yavuz, *Chem. Mater.* **2019**, *31*, 5206–5213; i) C. K. W. Meininghaus, R. Prins, *Microporous Mesoporous Mater.* **2000**, *35–36*, 349–365; j) M. C. Long, P. Liu, Y. Li, A. Li, Q. Zhang, *Environ. Sci. Technol.* **2011**, *45*, 4506–4512.

Manuscript received: December 5, 2024
Accepted manuscript online: January 13, 2025
Version of record online: January 21, 2025